Annals of Nuclear Medicine (2019) 33:404–413
https://doi.org/10.1007/s12149-019-01348-7

ORIGINAL ARTICLE

Preliminary results of biodistribution and dosimetric analysis of [^{68}Ga]Ga-DOTA^{ZOL}: a new zoledronate-based bisphosphonate for PET/CT diagnosis of bone diseases

Ambreen Khawar[1] · Elisabeth Eppard[1] · Frank Roesch[2] · Hojjat Ahmadzadehfar[1] · Stefan Kürpig[1] · Michael Meisenheimer[1] · Florian. C. Gaertner[1] · Markus Essler[1] · Ralph. A. Bundschuh[1]

Received: 27 December 2018 / Accepted: 25 February 2019 / Published online: 15 March 2019

Abstract

Objective Pre-clinical studies with gallium-68 zoledronate ([^{68}Ga]Ga-DOTA^{ZOL}) have proposed it to be a potent bisphosphonate for PET/CT diagnosis of bone diseases and diagnostic counterpart to [^{177}Lu]Lu-DOTA^{ZOL} and [^{225}Ac]Ac-DOTA^{ZOL}. This study aims to be the first human biodistribution and dosimetric analysis of [^{68}Ga]Ga-DOTA^{ZOL}.

Methods Five metastatic skeletal disease patients (mean age: 72 years, M: F; 4:1) were injected with 150–190 MBq (4.05–5.14 mCi) of [^{68}Ga]Ga-DOTA^{ZOL} i.v. Biodistribution of [^{68}Ga]Ga-DOTA^{ZOL} was studied with PET/CT initial dynamic imaging for 30 min; list mode over abdomen (reconstructed as six images of 300 s) followed by static (skull to mid-thigh) imaging at 45 min and 2.5 h with Siemens Biograph 2 PET/CT camera. Also, blood samples (8 time points) and urine samples (2 time points) were collected over a period of 2.5 h. Total activity (MBq) in source organs was determined using interview fusion software (MEDISO Medical Imaging Systems, Budapest, Hungary). A blood-based method for bone marrow self-dose determination and a trapezoidal method for urinary bladder contents residence time calculation were used. OLINDA/EXM version 2.0 software (Hermes Medical Solutions, Stockholm, Sweden) was used to generate residence times for source organs, organ absorbed doses and effective doses.

Results High uptake in skeleton as target organ, kidneys and urinary bladder as organs of excretion and faint uptake in liver, spleen and salivary glands were seen. Qualitative and quantitative analysis supported fast blood clearance, high bone to soft tissue and lesion to normal bone uptake with [^{68}Ga]Ga-DOTA^{ZOL}. Urinary bladder with the highest absorbed dose of 0.368 mSv/MBq presented the critical organ, followed by osteogenic cells, kidneys and red marrow receiving doses of 0.040, 0.031 and 0.027 mSv/MBq, respectively. The mean effective dose was found to be 0.0174 mSv/MBq which results in an effective dose of 2.61 mSv from 150 MBq.

Conclusions Biodistribution of [^{68}Ga]Ga-DOTA^{ZOL} was comparable to [^{18}F]NaF, [^{99m}Tc]Tc-MDP and [^{68}Ga]Ga-PSMA-617. With proper hydration and diuresis to reduce urinary bladder and kidney absorbed doses, it has clear advantages over [^{18}F]NaF owing to its onsite, low-cost production and theranostic potential of personalized dosimetry for treatment with [^{177}Lu]Lu-DOTA^{ZOL} and [^{225}Ac]Ac-DOTA^{ZOL}.

Keywords ^{68}Ga]Ga-DOTA^{ZOL} · Biodistribution · Theranostic radionuclides · Metastatic skeletal disease · Bronchial carcinoma

Background

Metastatic skeletal disease is a long known complication in many solid tumors. It affects up to 70% of patients suffering from advanced breast or prostate cancer. It is a major contributor to increased morbidity and mortality in these patients [1–3]. The role of nuclear medicine in diagnosis, staging and assessment of treatment response in these patients is well established. Among available SPECT and

✉ Ambreen Khawar
ambreen_khawar@hotmail.com

[1] Department of Nuclear Medicine, University Medical Center Bonn, Bonn, Germany

[2] Institute of Nuclear Chemistry, Johannes Gutenberg-University Mainz, Mainz, Germany

PET tracers, [^{18}F]NaF PET/CT has shown sensitivity of 100% and specificity of 97% [4]. Using β^- and α-emitting radionuclides for pain palliation in these patients has proved beneficial [5]. The theranostic role of nuclear medicine for management of skeletal metastatic disease has progressed from pain palliation to delivery of targeted cytotoxic radionuclide therapy as is seen with prostate-specific membrane antigen (PSMA) targeted therapies for prostate carcinoma [6]. However, targeted therapies for skeletal metastasis secondary to other tumor entities are still being investigated.

Since many years, bisphosphonates have been used for pain palliation and prevention of complications from skeletal metastases. Their anti-resorptive effect has been proven in vivo and in vitro fact [7]. The high rate of adsorption by bisphosphonates encouraged its labeling with theranostic radionuclides [8]. Success in this regard has been found in successful development of ^{99m}Tc-labeleld bisphosphonates such as [^{99m}Tc]Tc-Alendronate [9] and various acyclic bisphosphonates such as, e.g., EDTMP [ethylenediamine tetra (methylene phosphonic acid] labeled with trivalent ^{68}Ga and ^{177}Lu such as [^{68}Ga]Ga-EDTMP [10], and [^{177}Lu]Lu-EDTMP [11–15]. In addition, there is a class of bisphosphonates conjugated to macrocyclic chelators, which allow for labeling with trivalent radiometals [16, 17]. Among this group, simple bisphosphonates have been investigated first such as BPAMD (4-{[(bis(phophonomethyl)carbamoyl] methyl}-7,10-bis(carboxymethyl)-1,4,7,10-tetraazacyclododec-1-yl) acetic acid, resulting in [^{68}Ga]Ga-BPAMD [18] and [^{177}Lu]Lu-BPAMD [18, 19]. Despite the great potential of BPAMD as a theranostic pair, further radiopharmaceutical research demonstrated, that the NOTA version [^{68}Ga]Ga-NO2AP^{BP} (^{68}Ga-1,4,7-triazacyclonone-1,4-diacetic acid) of that bisphosphonate not only allowed for more effective labelling with ^{68}Ga, but also demonstrated superior targeting quality [20]. It is superior with high thermodynamic stability and kinetic inertness as compared to DOTA-labeled ^{68}Ga bisphosphonates, labeling of which is less efficient and more vulnerable to experimental conditions. It was characterized by high skeletal uptake and less kidney uptake [20]. However, in pre-clinical animal biodistribution studies, its therapeutic counterpart [^{177}Lu]Lu-NO2AP^{BP} was found inferior to [^{177}Lu]Lu-BPAMD with less affinity to skeleton [21]. To date, [^{68}Ga]Ga-NO2AP^{BP} and [^{177}Lu]Lu-BPAMD thus represent the theranostic combination of the simple bisphosphonate.

Alpha-hydroxy bisphosphonates like pamidronate and, in particular, alpha-hydroxy bisphosphonates containing a potent nitrogen-containing moiety like zoledronate represent the next generation of bisphosphonates [22–24]. In addition to binding with hydroxyapatite structure of the bone, their interaction with the HMG CoA reductase pathway results in inhibition of farnesyl diphosphate synthase (FPPS) culminating in apoptosis of osteoclasts, hence exhibiting a biochemical target [8]. Among them, zoledronic acid has shown the highest FPPS inhibition and best affinity to hydroxyl apatite making it the bisphosphonate of choice for labeling with diagnostic and therapeutic radionuclide [24]. The bifunctional chelate DOTA has facilitated labeling of these bisphosphonates with Me (III), ^{68}Ga and ^{177}Lu [17] for diagnosis and treatment of skeletal metastatic disease, respectively, thus achieving a chemical goal of new theranostic development [17].

Pre-clinical in vitro and in vivo studies with [^{68}Ga]Ga-DOTA^{ZOL} have shown high hydroxyapatite binding, good target to background ratio with fast renal clearance and overall skeletal uptake comparable to other ^{68}Ga-labeled DOTA α-H and α-OH bisphosphonates as well as [^{18}F]Na-F [16, 17]. Moreover, in vivo biodistribution in a single patient with prostatic carcinoma showed intense uptake in skeletal metastatic lesions with lower activity in background and other normal organs in comparison with complimentary [^{68}Ga]Ga-PSMA image [16]. Recently, pre-clinical animal studies with alpha emitter [^{225}Ac]Ac-DOTA^{ZOL} [25] have shown biokinetics similar to [^{68}Ga]Ga-DOTA^{ZOL} and proposed its translational use with strategies to reduce nephrotoxicity, thus increasing the importance of theranostic use of [^{68}Ga]Ga-DOTA^{ZOL}.

Literature-based comparison of [^{68}Ga]Ga-DOTA^{ZOL} [17] with [^{68}Ga]Ga-NO2AP^{BP} [20] revealed slightly less hydroxyapatite binding ($92.7 \pm 1.3\%$ versus $93.8 \pm 4.4\%$) and low bone uptake at 60 min p.i. (standard uptake value (SUV) of 5.27 ± 0.62 versus 6.19 ± 1.27). The in vivo biodistribution of [^{68}Ga]Ga-DOTA^{ZOL} in male Wistar rats showed faster kidney clearance with peak uptake in less than 5 min followed by clearance in comparison to [^{68}Ga]Ga-NO2AP^{BP} that showed continuous uptake till 50 min followed by clearance through urinary bladder [20]. However, SUV for kidneys at 60 min p.i was found to be higher for [^{68}Ga]Ga-DOTA^{ZOL} (0.53 ± 0.04) as compared to [^{68}Ga]Ga-NO2AP^{BP} (0.26 ± 0.09). Evaluation of [^{68}Ga]Ga-NO2AP^{BP} in female breast carcinoma patients already proved its excellent ability to detect lesions along with favorable radiation dosimetry with very low kidney absorbed dose [26]. However, [^{68}Ga]Ga-DOTA^{ZOL} has not been evaluated clinically so far.

[^{68}Ga]Ga-DOTA^{ZOL} with benefit of low cost, onsite generator production of gallium-68 [27], having biodistribution and skeletal uptake comparable with [^{177}Lu]Lu-DOTA^{ZOL} [17, 25] and [^{225}Ac]Ac-DOTA^{ZOL} [25] suggests it to be better than[^{18}F]Na-F as potential theranostic tracer allowing for patient-individual dosimetry. In this study, we evaluated human biodistribution and radiation dosimetry with [^{68}Ga]Ga-DOTA^{ZOL}.

Materials and methods

It is stated that [^{68}Ga]Ga-DOTA^{ZOL} was applied to the patients within an individual treatment attempt according to German drug regulations. The data were evaluated afterwards retrospectively. All procedures were followed in accordance with ethical standards of our institutional review board and therefore been performed in accordance with the ethical standards laid down in the 1964 Declaration of Helsinki and all subsequent revisions. All patients gave their informed consent prior to their inclusion in the study.

Patient population

Between April 2016 to March 2018, 5 patients (M: F; 4: 1) with metastatic skeletal disease not responding to other treatment modalities were included in this study (Table 1). The patients were injected intravenously (i.v.) with mean ± SD dose of 168.25 ± 20.27 MBq (4.55 mCi) of [^{68}Ga]Ga-DOTA^{ZOL}. Skeletal metastatic disease in patients was secondary to breast, bronchial and metastatic castration-resistant prostate carcinoma (mCRPC). All of these patients had shown painful progression while being treated with conventional treatment modalities.

Preparation of [^{68}Ga]Ga-DOTA^{ZOL}

Gallium-68 was obtained from a 1.85 GBq (50 mCi) ^{68}Ge/^{68}Ga generator (iThemba Labs; South Africa). Radiolabeling was performed according to the method described by Meckel et al. [17]. Development of silica TLC plates was conducted in acetylacetone/acetone (1:1) for iTLC plates. A radiochemical yield of ≥ 98% and radiochemical purity of ≥ 97% were obtained.

[^{68}Ga]Ga-DOTA^{ZOL} PET/CT imaging protocol

For qualitative and dosimetric analysis, a Siemens Biograph 2 PET/CT scanner with a 58.5 cm axial field of view and a 16.2 cm longitudinal field of view was used for acquiring PET/CT images. The scanner has a spatial resolution of about 6 mm in axial and transversal direction (at a radius of 10 mm). All patients underwent a low-dose CT scan (120 kV, 40mAs) of abdomen for attenuation correction and patient positioning with kidneys in field of view, followed by dynamic imaging of abdomen for 30 min in list mode started simultaneously with i.v. injection of [^{68}Ga]Ga-DOTAZOL. Later, static skull to mid-thigh PET/CT images were acquired at 45 min and 2.5 h post-injection (p.i), each preceded by low-dose CT examination for patient positioning and attenuation correction. Images were reconstructed using an iterative reconstruction algorithm (OSEM with 8 iterations, 16 subsets), application of Gaussian filter of 4 mm and were corrected for scatter. The dynamic images were reconstructed into 6 images of 300 s.

Qualitative analysis

All dynamic and static images were visually analyzed to see physiological and pathological tracer distribution. Organs with increased tracer uptake were identified as source organs for further dosimetric analysis.

Quantitative dosimetric analysis

For dosimetric analysis kidneys, liver, spleen, urinary bladder, lumbar (L1-L3) vertebrae, salivary glands and whole body were selected as source organs. MEDISO interview fusion software (MEDISO Medical Imaging

Table 1 Characteristics of study population

	PT1	PT2	PT3	PT4	PT5	Mean	SD
Age	83	83	66	64	64	72	10.07
Weight	76	76	85	82	82	80	4.02
Sex	M	M	F	M	M		
Hematocrit	0.4	0.41	0.34	0.39	0.37	0.38	0.03
Dose	152	150	181	190	190	172.60	20.07
Tumor	mCRPC	mCRPC	Breast	Bronchial carcinoma	Bronchial carcinoma		
Previous therapies received	AH[a]/ CT[b]/ [^{177}Lu]Lu-PSMA-617	AH[a]/ CT[b]/ [^{177}Lu]Lu-PSMA-617	CT[b] + local irradiation	CT[b]/ denosumab, nivolumab	CT[b]/ denosumab, nivolumab		

[a]Antihormonal

[b]Chemotherapy

Systems, Budapest, Hungary) was used to draw a volume of interest (VOI) encompassing the entire source organs on CT image for calculating organ volume and to determine mean counts/ml (kBq/ml) from a co-registered PET image. Total source organ activity (MBq) was calculated by multiplying source organ CT volume with corresponding mean counts/ml and dividing it with 1000. The percent of injected activity in source organs was calculated to generate time activity curves and calculating residence time (MBq-h/MBq) using OLINDA/EXM version 2.0 (Hermes Medical Solutions, Stockholm, Sweden). Mono-exponential curve was fit on whole body and salivary glands. Bi-exponential curve was applied for the remaining source organs. Assuming homogenous distribution of tracer in the remainder of the body, the percentage of injected dose in the image was scaled proportional to percentage weight of body in the image by using Eq. (1) [28]. The percentage of body weight in image was calculated using Eq. (2) [28].

$$\%\text{Whole body Activity}(t) = \frac{\text{Activity in static (skull} - \text{midthigh)image } (t) \times 100}{\text{Scaled injected activity in image}} \quad (1)$$

$$\%\text{Body weight(image)} = \frac{\text{CT volume of whole bodyimage} \times \text{mean CT density} \times 100}{\text{Patient weight}} \quad (2)$$

For the remainder of body activity $A \times [1 - \exp^{-\lambda t}]$ function was fit for cumulative urinary excretion using the method explained by Stabin [29]. For skeletal activity, the mean counts/ml in lumbar vertebrae were multiplied by 5000 (total weight of skeleton in an adult) [30].

To determine bone marrow dosimetry, 1–2 ml venous blood samples were collected at eight time points (5, 10, 15, 20, 25, 30, 45 min and 2.5 h) post-injection. Urine samples were also collected in pre-weighed containers after 45 min and 2.5 h p.i. Radioactivity in 1 ml blood and urine samples was measured along with known standard activity using 1480 WIZARD™ 3n Gamma counter. The indirect blood-based method using patient hematocrit-based red marrow to blood ratio and bone marrow mass was used to determine bone marrow self-dose [31–34]. For urinary bladder contents residence time, a trapezoidal method was used while taking into account urinary bladder activity in images at 45 min, and 2.5 h along with activity in urinary samples. OLINDA/EXM version 2.0 (Hermes Medical Solutions, Stockholm, Sweden) software was used to calculate mean organ absorbed doses and effective doses after adjusting for the weight of patient organs by multiplying the reference adult male/female whole body weight with factor obtained by dividing patient weight with reference adult (male/female) weight, respectively.

The mean of residence times, organ absorbed doses (mSv/MBq) and mean effective doses (mSv/MBq) were calculated. The total effective dose in mSv received after injection of 150 MBq of [^{68}Ga]Ga-DOTA^{ZOL} was calculated by multiplying the mean effective dose (mSv/MBq) with 150 MBq.

Results

Qualitative [^{68}Ga]Ga-DOTA^{ZOL} distribution and kinetics analysis

Visual analysis of PET/CT images revealed intense tracer uptake in kidneys, skeleton and urinary bladder. Faint uptake in liver, spleen and salivary glands was also seen. Rapid tracer kinetics was seen through kidneys as shown in Fig. 1 with early uptake in renal parenchyma as early as 2.5 min followed by clearance with minimal activity in the collecting system at 45 min p.i.. and minimal to no residual activity at 2.5 h p.i.. Uptake in bone increased over time. Good bone to soft tissue and metastatic lesion to normal bone uptake was visualized at 45 min p.i.. which increased at 2.5 p.i. as seen in Fig. 2. For dosimetric analysis, source organs identified on qualitative analysis included kidneys, urinary bladder, lumbar vertebrae (L1–L3) as representative of skeletal system, liver, spleen, salivary glands and whole body.

Comparison of mean SUV-based skeletal to soft tissue ratio was found to be 7.36 and 12.96 at 45 min p.i. that increased to 15.034 and 28.82 at 2.5 h p.i. for two representative lesions as shown in Fig. 2 in comparison to 4.81 and 3.30 on previous [^{68}Ga]Ga-PSMA-617 in a patient with mCRPC. Lesion to normal bone ratio for these lesions was found to be 7.53 and 12.95 at 45 min and 6.79 and 13.01 at 2.5 h p.i.. on PET/CT images of [^{68}Ga]Ga-DOTA^{ZOL} in comparison to 7.5 and 5.14, respectively, on the [^{68}Ga]Ga-PSMA-617 image. The number of lesions was also higher on [^{68}Ga]Ga-DOTA^{ZOL} as compared to [^{68}Ga]Ga-PSMA-617 in the mCRPC patient.

Visual comparison of [^{68}Ga]Ga-DOTA^{ZOL} with [^{18}F]FDG in bronchial carcinoma patients and [^{99m}Tc]Tc-MDP bone scan in the female patient as shown in Figs. 3 and 4, respectively, also revealed that uptake in lesions and the apparent number of lesions were also higher. SUV max in lesion was

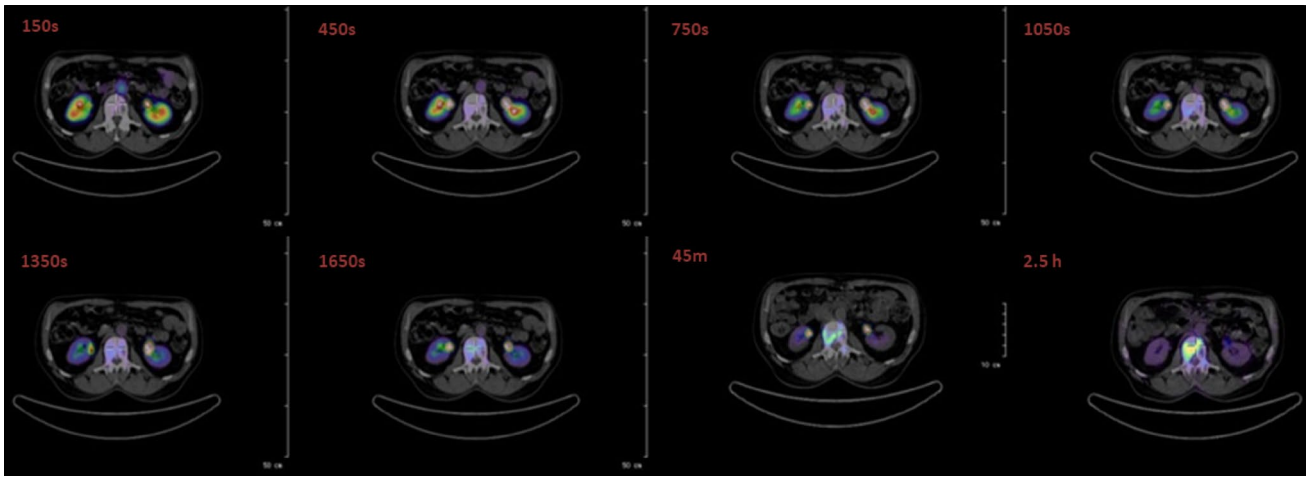

Fig. 1 [^{68}Ga]Ga-DOTA^{ZOL} kinetics through kidneys in dynamic (150 s, 450 s, 750 s, 1050s, 1350s, 1650s) and static images (45 min and 2.5 h)

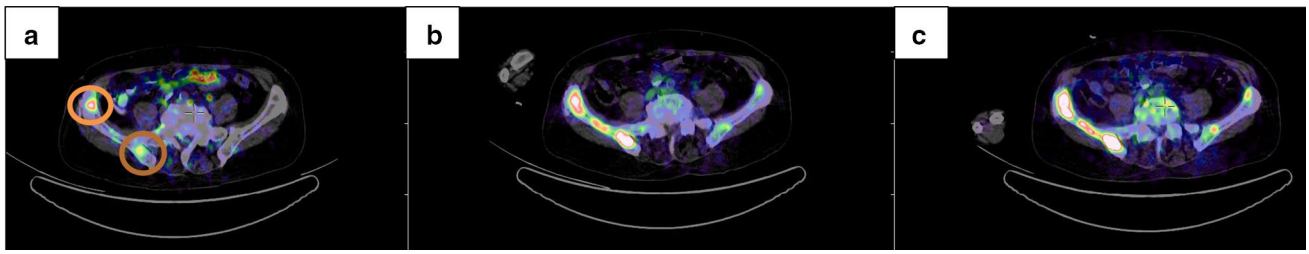

Fig. 2 Uptake in two metastatic lesions on **a**. [^{68}Ga]Ga-PSMA-617, **b**. [^{68}Ga]Ga-DOTA^{ZOL} at 45 min p.i.. and **c**. [^{68}Ga]Ga-DOTA^{ZOL} at 2.5 h p.i.. showing higher and progressive uptake with [^{68}Ga]Ga-DOTA^{ZOL} as a result of enhanced lesion to normal bone uptake

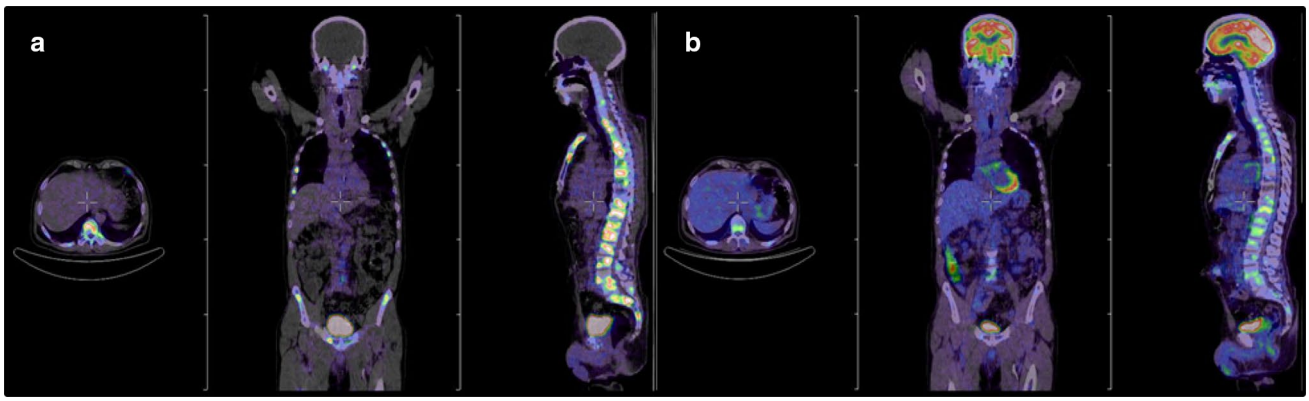

Fig. 3 Comparison of PET/CT images of **a**. [^{68}Ga]Ga-DOTA^{ZOL} with **b**. [^{18}F]FDG in patient with skeletal metastases secondary to bronchial carcinoma.

also higher on [^{68}Ga]Ga-DOTA^{ZOL} (15.24 g/ml) as compared to [^{18}F]FDG PET/CT images (5.95 g/ml) in bronchial carcinoma patients.

Dosimetric analysis for normal organs

Plotting of percentage injected activity in source organs with respect to time as shown in Figs. 5 and 6 further supported the results of visual analysis. The highest tracer localization was seen in the skeletal system followed by liver, kidneys,

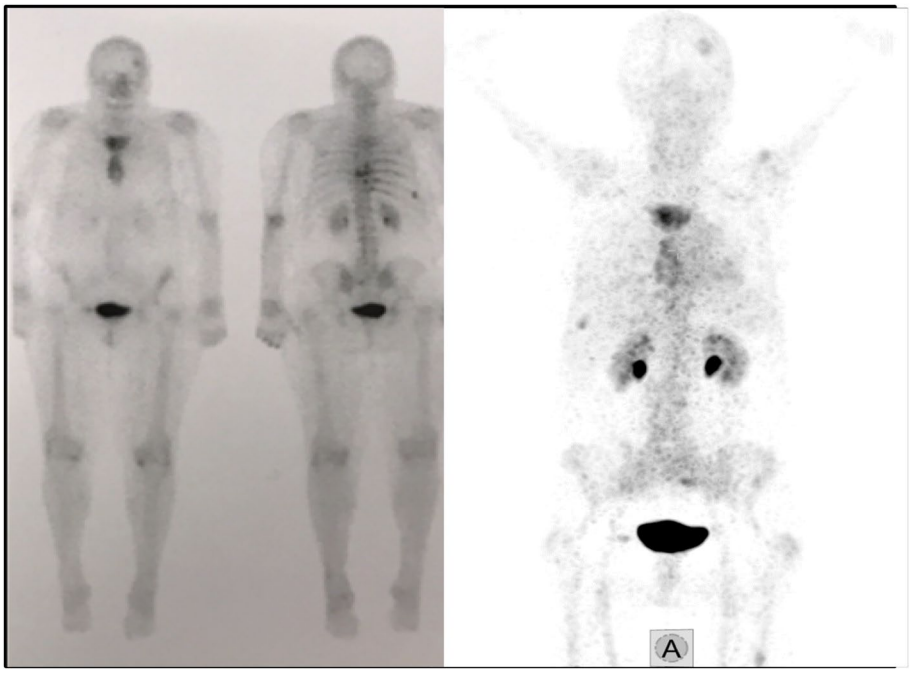

Fig. 4 Comparison of [^{99m}Tc] Tc-MDP with [^{68}Ga]Ga-DOTA-^{ZOL} in patient with skeletal metastases secondary to breast carcinoma

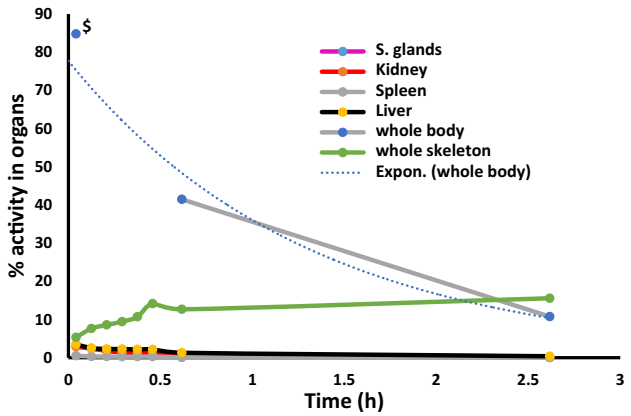

Fig. 5 Tracer kinetics of [^{68}Ga]Ga-DOTA^{ZOL} in source organs with decay correction and $(estimated initial activity)

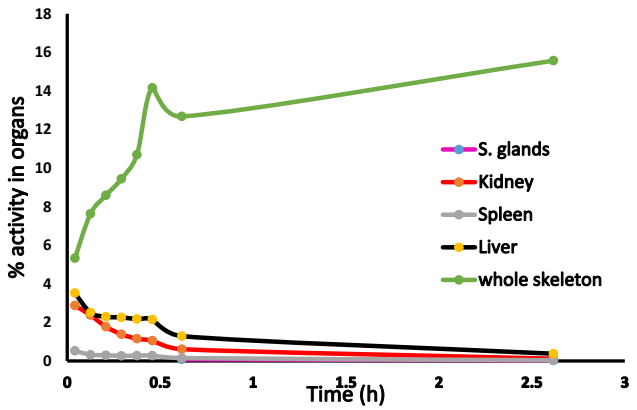

Fig. 6 Change in percentage of activity of [^{68}Ga]Ga-DOTA^{ZOL} in whole skeleton (with decay correction) and remaining source organs (without decay correction)

spleen and salivary glands. An initial rapid increase uptake was seen in the skeleton for almost half an hour p.i. followed by a slow rise. Simultaneous rapid tracer uptake and fast washout in the other source organs and blood pool was found. Rapid tracer kinetics with early peak physiological uptake as early as 2.5 min p.i. was seen in kidneys, followed by fast clearance with minimal to almost no activity at 2.5 h p.i.. Almost 11% of the injected activity remained in whole body at 2.5 h showing 89% renal excretion.

Table 2 shows the residence times (MBq-h/MBq) for source organs in individual patients as well as the mean ± SD of residence times. High residence time was seen in the remainder of the body followed by urinary bladder, cortical and trabecular bone, liver, red marrow, kidneys, spleen and salivary glands. Table 3 shows mean ± SD and ranges of organ absorbed doses as well as effective dose according to ICRP103. The results very clearly demonstrate that the urinary bladder receives the highest dose of 0.368 mSv/ MBq (range 0.203–0.609 mSv/ MBq) and is the organ at risk as kidneys were found to be the only route of its excretion. Osteogenic cells received dose of 0.040 mSv/MBq followed by kidneys (0.031 mSv/ MBq), red marrow (0.027 mSv/MBq), spleen (0.018 mSv/ MBq), liver (0.013 mSv/MBq) and salivary glands (0.011 mSv/MBq).

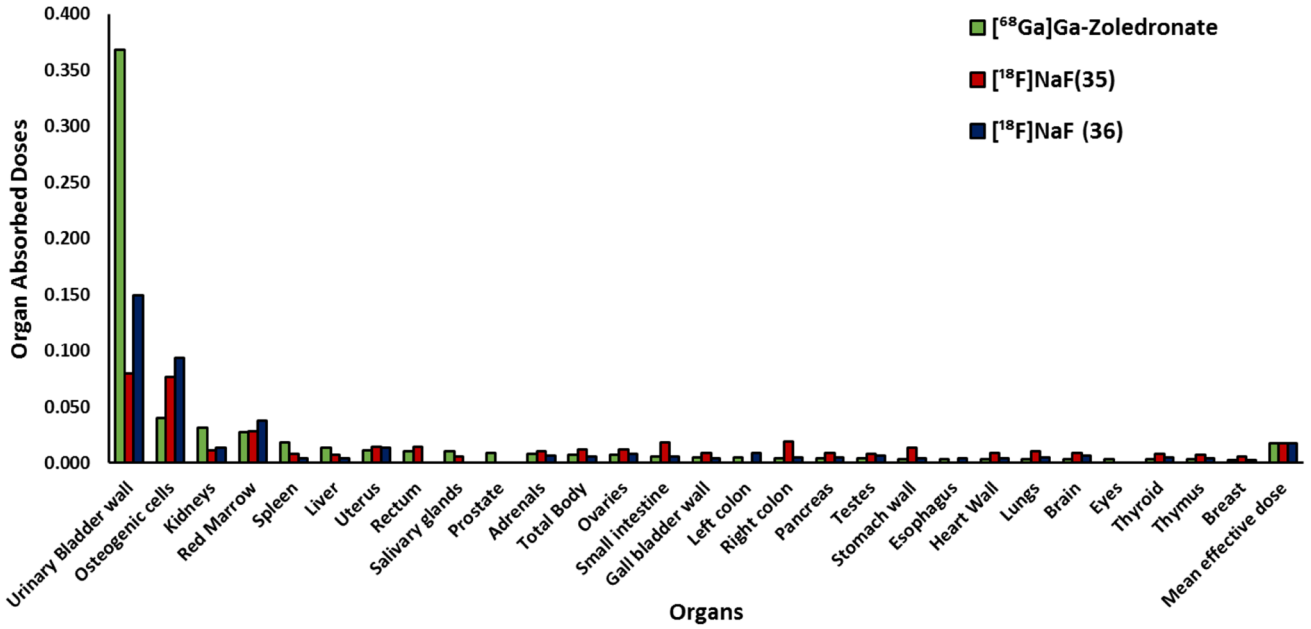

Fig. 7 Comparison of organ absorbed doses between [^{68}Ga]Ga-DOTA^{ZOL} and [^{18}F]NaF (35, 36)

Table 2 Comparison of residence time (MBq-h/ MBq) in source organs with [^{68}Ga]Ga-DOTA^{ZOL} and [^{18}F]NaF

Organs	[^{68}Ga]Ga-DOTA^{ZOL} this study							Mean	
	PT 1	PT 2	PT 3	PT 4	PT 5	mean	± SD	[^{18}F]NaF [35]	[^{18}F]NaF [36]
S. glands	0.004	0.002	0.001	0.001	0.001	0.002	0.001		
Kidney	0.024	0.024	0.020	0.018	0.016	0.021	0.003	0.010	
Spleen	0.005	0.004	0.008	0.004	0.006	0.005	0.001	0.002	
Liver	0.057	0.034	0.052	0.028	0.032	0.040	0.012	0.017	
Red marrow	0.034	0.038	0.053	0.039	0.058	0.042	0.009	0.130	
Trabecular Bone	0.148	0.117	0.116	0.225	0.150	0.127	0.041	0.207	0.830
Cortical bone	0.148	0.117	0.116	0.225	0.150	0.127	0.041	0.901	0.550
Urinary Bladder	0.172	0.191	0.160	0.534	0.496	0.174	0.177	0. 190	0.290
Remainder of body	0.392	0.468	0.213	0.251	0.377	0.358	0.095		0.330

Discussion

In the current study, [^{68}Ga]Ga-DOTA^{ZOL} was evaluated in bronchial carcinoma patients in addition to mCRPC and breast carcinoma patients. [^{68}Ga]Ga-DOTA^{ZOL} showed fast kinetics with increased tracer elimination through kidneys resulting in whole body activity to decrease to almost 11% by 2.5 h p.i. In the skeletal target organ, there is an initial rapid uptake till 30 min followed by a further gradual rise. The maximum tracer accumulation was seen in the skeletal system with 18% of injected activity (IA) in one of the bronchial carcinoma patients with a high burden of skeletal metastases.

An initial uptake in liver, spleen and salivary glands was also seen followed by a sharp decline. Soft tissue and blood activity decreases with time and results in enhanced bone uptake and an increased metastatic lesion to bone ratio as can be seen in Fig. 2 which is consistent with the results of other ^{68}Ga–bisphosphonate agents and [^{18}F]NaF [17, 27].

PET/CT images of [^{68}Ga]Ga-DOTA^{ZOL} could be compared to previous [^{68}Ga]Ga-PSMA-617 and [^{18}F]FDG PET/CT images in the male patients and a [^{99m}Tc]Tc-MDP bone scan enrolled in this study. Here, the uptake of [^{68}Ga]Ga-DOTA^{ZOL} was 2.56 times higher than that of [^{18}F]FDG in a bronchial carcinoma patient. A greater number of apparent lesions was also found with [^{68}Ga]Ga-DOTA^{ZOL} as

Table 3 Organ absorbed doses (mSv/MBq) and effective dose(mSv) from 150 MBq

	PT 1	PT 2	PT 3	PT 4	PT 5	Mean	SD
Organs							
Adrenals	9.24E−03	6.59E−03	9.68E−03	6.25E−03	7.27E−03	7.81E−03	1.56E−03
Brain	4.29E−03	2.23E−03	3.22E−03	3.05E−03	3.82E−03	3.32E−03	7.85E−04
Breast			2.65E−03			2.65E−03	
Esophagus	4.64E−03	2.38E−03	3.65E−03	3.01E−03	4.04E−03	3.54E−03	8.80E−04
Eyes	4.27E−03	2.22E−03	3.23E−03	3.06E−03	3.83E−03	3.32E−03	7.82E−04
Gall bladder wall	6.54E−03	3.57E−03	4.72E−03	3.87E−03	5.21E−03	4.78E−03	1.18E−03
Left colon	5.30E−03	3. 02E−03	4.56E−03	4.19E−03	5.37E−03	4.49E−03	9.60E−04
Small intestine	5.67E−03	3.45E−03	4.72E−03	5.53E−03	6.79E−03	5.23E−03	1.24E−03
Stomach wall	4.65E−03	2.34E−03	3.91E−03	2.86E−03	4.10E−03	3.57E−03	9.46E−04
Right colon	5.25E−03	2.81E−03	4.01E−03	4.03E−03	5.28E−03	4.28E−03	1.03E−03
Rectum	8.19E−03	6.31E−03	1.14E−02	1.27E−02	1.39E−02	1.05E−02	3.17E−03
Heart wall	4.72E−03	2.37E−03	3.46E−03	2.92E−03	4.09E−03	3.51E−03	9.29E−04
Kidneys	3.67E−02	3.66E−02	3.52E−02	2.48E−02	2.36E−02	3.14E−02	6.59E−03
Liver	1.75E−02	1.06E−02	2.01E−02	8.15E−03	9.80E−03	1.32E−02	5.24E−03
Lungs	4.52E−03	2.30E−03	3.64E−03	2.86E−03	3.92E−03	3.45E−03	8.76E−04
Ovaries			6.91E−03			6.91E−03	
Pancreas	5.22E−03	2.78E−03	4.88E−03	3.45E−03	4.67E−03	4.20E−03	1.04E−03
Prostate	9.57E−03	7.90E−03		1.68E−02	1.80E−02	8.74E−03	1.18E−03
Salivary glands	2.16E−02	1.07E−02	6.51E−03	4.75E−03	6.56E−03	1.00E−02	6.83E−03
Red marrow	2. 65E−02	2.20E−02	3.02E−02	2.91E−02	2.83E−02	2.72E−02	3.22E−03
Osteogenic cells	4.19E−02	3.38E−02	3.51E−02	4.86E−02	4.06E−02	4.00E−02	5.92E−03
Spleen	1.71E−02	1.34E−02	2.93E−02	1.25E−02	1.75E−02	1.80E−02	6.71E−03
Testes	5.02E−03	3.11E−03		5.60E−03	6.68E−03	4.07E−03	1.35E−03
Thymus	4.14E−03	1.99E−03	3.10E−03	2.54E−03	3.65E−03	2.94E−03	9.18E−04
Thyroid	4.26E−03	2.10E−03	3.06E−03	2.78E−03	3.79E−03	3.20E−03	8.48E−04
Urinary bladder wall	2.03E−01	2.22E−01	2.35E−01	6.09E−01	5.72E−01	3.68E−01	2.04E−01
Uterus			1.14E−02			1.14E−02	
Total body	8.20E−03	5.75E−03	7.68E−03	6.92E−03	7.47E−03	7.20E−03	9.33E−04
Effective dose (150 MBq)	2.61 mSv						

compared to [^{68}Ga]Ga-PSMA-617 (Fig. 2), [^{18}F]FDG in bronchial carcinoma (Fig. 3) and [^{99m}Tc]Tc-MDP in breast carcinoma patients (Fig. 4).

Compared with [^{68}Ga]Ga-PSMA-617, the qualitative analysis of [^{68}Ga]Ga-DOTA^{ZOL} showed better uptake in skeleton with higher skeleton to soft tissue and metastatic lesions to normal bone ratio as seen in Fig. 2. This finding is consistent with the in vivo biodistribution analysis of [^{68}Ga]Ga-DOTA^{ZOL} in one patient with prostate cancer [16].

Dosimetric analysis showed comparable residence times for the rest remainder of the body to that of [^{18}F]NaF which was 0.358 h in the current study and 0.33 reported in ICRP 106 report. Urinary bladder residence time (0.174 h) was found to be less than that of [^{18}F]NaF (0.19 and 0.29 h); however, the residence time for kidneys was found to be higher (0.022 h) as compared to [^{18}F]NaF (0.01 h). This could be explained by the fact that [^{68}Ga]Ga-DOTA^{ZOL} shows 89% renal excretion over a period of 2.5 h as compared to 15% and 50% in the case of [^{18}F]NaF [35, 36]. The residence time of [^{68}Ga]Ga-DOTA^{ZOL} in trabecular and cortical bone was found to be 0.127 with 50% weightage given to both. The residence time in bone components as well as bone marrow was lower as compared to [^{18}F]NaF. This might be a result of the lower half-life of ^{68}Ga as compared to ^{18}F as well as the difference in osteogenic tumor load in patients evaluated by Kurdziel et al. [35] and the current study. Residence times for liver and spleen were higher than those of [^{18}F]NaF. The uptake of free/unbound ^{68}Ga can be responsible for prolonged residence times in these organs.

[^{68}Ga]Ga-DOTA^{ZOL} like other bone-seeking agents was found to be characterized by delivery of the highest radiation absorbed dose to urinary bladder, followed by osteogenic cells, red marrow and kidneys. This finding is comparable with dosimetric analysis of [^{18}F]NaF [35, 36]. Kidney being its physiological route of excretion results in the highest dose seen in urinary bladder. The doses

Table 4 Comparison of organ absorbed doses of [^{68}Ga]Ga-NO2AP^{BP} [27] with [^{68}Ga]Ga-DOTA^{ZOL}

Study	[^{68}Ga]Ga-NO2AP^{BP}	[^{68}Ga]Ga-DOTA^{ZOL}
Organs	Organ absorbed doses(mSv/MBq)	
Kidneys	0.00760	0.0314
Red marrow	0.02030	0.0272
Urinary bladder	0.00011	0.3680
Skeleton	0.05800	0.0400
Whole body	0.00583	0.0072
Mean effective dose	0.00860	0.0174

delivered to urinary bladder and kidneys were higher and the radiation absorbed doses to osteogenic tissue and red marrow were lower as compared to [^{18}F]NaF as shown in Fig. 7 [35, 36]. Mean effective dose and total effective dose were found to be 0.017 mSv/MBq and 2.61 mSv with [^{68}Ga]Ga-DOTA^{ZOL} comparable to 0.017 mSv/MBq and 1.88–3.15 mSv with [^{18}F]NaF respectively [35].

Comparison of dosimetric analysis of [^{68}Ga]Ga-DOTA-^{ZOL} with [^{68}Ga]Ga-NO2AP^{BP} [26] revealed high absorbed doses delivered to kidneys and urinary bladder, almost comparable absorbed doses to bone marrow and osteogenic cells, high total body absorbed dose and high effective dose equivalent as shown in Table 4 which illustrates the superiority of [^{68}Ga]Ga-NO2AP^{BP} [26]. The difference in kidney and urinary bladder absorbed doses could be due to differences in the collection of data points till 4 h for [^{68}Ga]Ga-NOTAP^{BP} in comparison to 2.5 h in the current study. A further lack of detailed biodistribution analysis is also a limitation for comparing the results of the two studies. It was observed that the dosimetric results of [^{68}Ga]Ga-NO2AP^{BP} from breast carcinoma patients (M:F; 1:4) were not comparable to the results for the one female breast carcinoma patient (Pt 3) in the current study.

The resultant high urinary bladder and kidney absorbed doses from [^{68}Ga]Ga-DOTA^{ZOL} are consistent with those of other bone-seeking agents. These doses can very easily be reduced by proper hydration and rapid diuresis. As compared to various ^{68}Ga-labeled octreotide [37] and PSMA agents [38, 39], [^{68}Ga]Ga-DOTA^{ZOL} delivered lower kidney and higher urinary bladder absorbed doses along with lower mean effective doses. Besides having high radiation exposure to kidneys and urinary bladder, [^{68}Ga]Ga-DOTA^{ZOL} has advantages of its theranostic potential when labeled with ^{177}Lu for therapy.

Conclusions

The results of this small patient study showed that [^{68}Ga]Ga-DOTA^{ZOL} is an excellent tracer with high and selective uptake in bone lesions. [^{68}Ga]Ga-DOTA^{ZOL} results in 2.4 times higher organ absorbed dose to urinary bladder and kidneys, while similar mean effective dose in comparison to that of [^{18}F]NaF which was found to be 0.017 mSv/MBq. Compared with [^{68}Ga]Ga-PSMA-617, the bisphosphonate [^{68}Ga]Ga-DOTA^{ZOL} showed a similar pharmacological pattern as well as higher metastatic to normal bone ratio and higher skeleton to soft tissue uptake in prostate carcinoma.

The possibility of treatment of bone metastases with [^{177}Lu]Lu-DOTA^{ZOL} gives it a clear advantage over other bone-seeking diagnostic agents such as [^{18}F]Na-F and [^{99m}Tc]Tc-MDP. These initial results are encouraging and support the use of [^{68}Ga]Ga-DOTA^{ZOL} as an imaging theranostic agent. However, prospective patient studies are required to explore its further potential for the treatment of bone metastases in different tumor entities.

Author contributions The manuscript has been seen and approved by all authors. AK, MM, SK,EE: contributed equally in design and execution of study. AK, FR, HA, ME, RAB, FCG: contributed in drafting or revising of the manuscript critically for important intellectual content as well as final manuscript approval for submission and publication.

Funding None.

Compliance with ethical standards

Conflict of interest None of the authors have any potential conflicts of interest to disclose.

References

1. Gonzalez-Sistal A, Baltasar A, Herranz M, Ruibal A. Advances in medical imaging applied to bone metastases. In: Medical Imaging. InTech; 2011. http://www.intechopen.com/books/medical-imaging/advances-in-medical-imaging-applied-to-bone-metastases. Accessed 14 July 2017.
2. Agarwal M, Nayak P. Management of skeletal metastases: an orthopaedic surgeon′s guide. Indian J Orthop. 2015;49:83–100.
3. Ulmert D, Solnes L, Thorek DL, Beyer T, Fujii T, Mochizuki T. Contemporary approaches for imaging skeletal metastasis. Bone Res. 2015;3:15024.
4. O'Sullivan GJ, Carty FL, Cronin CG. Imaging of bone metastasis: an update. World J Radiol. 2015;7:202–11.
5. Damerla V, Packianathan S, Boerner PS, Jani AB, Vijayakumar S, Vijayakumar V. Recent developments in nuclear medicine in the management of bone metastases: a review and perspective. Am J Clin Oncol Cancer Clin Trials. 2005;28:513–20.
6. Chatalic KLS, Heskamp S, Konijnenberg M, Molkenboer-Kuenen JDM, Franssen GM, Clahsen-van Groningen MC, et al. Towards

personalized treatment of prostate cancer: PSMA I&T, a promising prostate-specific membrane antigen-targeted theranostic agent. Theranostics. 2016;6:849–61.
7. Luckman SP, Hughes DE, Coxon FP, Russell RGG, Rogers MJ. Nitrogen-containing bisphosphonates inhibit the mevalonate pathway and prevent post-translational prenylation of GTP-binding proteins, including ras. J Bone Miner Res. 1998;13:581–9.
8. Fellner M, Biesalski B, Bausbacher N, Kubícek V, Hermann P, Rösch F, et al. 68 Ga-BPAMD: PET-imaging of bone metastases with a generator based positron emitter. Nucl Med Biol. 2012;39:993–9.
9. Ogawa K, Ishizaki A. Well-designed bone-seeking radiolabeled compounds for diagnosis and therapy of bone metastases. Biomed Res Int. 2015;2015:676053.
10. Fellner M, Riss P, Loktionova N, Zhernosekov K, Thews O, Geraldes CFGC, et al. Comparison of different phosphorus-containing ligands complexing ^{68}Ga for PET-imaging of bone metabolism. Radiochim Acta. 2011;99:43–51.
11. Agarwal KK, Singla S, Arora G, Bal C. 177Lu-EDTMP for palliation of pain from bone metastases in patients with prostate and breast cancer: a phase II study. Eur J Nucl Med Mol Imaging. 2015;42:79–88.
12. Alavi M, Omidvari S, Mehdizadeh A, Jalilian AR, Bahrami-Samani A. Metastatic bone pain palliation using ^{177}Lu-ethylenediaminetetramethylene phosphonic acid. World J Nucl Med. 2015;14:109–15.
13. Mazzarri S, Guidoccio F, Mariani G. The emerging potential of 177Lu-EDTMP: an attractive novel option for radiometabolic therapy of skeletal metastases. Clin Trans Imaging. 2015;3:167–8.
14. Shinto AS, Shibu D, Kamaleshwaran KK, Das T, Chakraborty S, Banerjee S, et al. ^{177}Lu-EDTMP for treatment of bone pain in patients with disseminated skeletal metastases. J Nucl Med Technol. 2014;42:55–61.
15. Yuan J, Liu C, Liu X, Wang Y, Kuai D, Zhang G, et al. Efficacy and safety of 177Lu-EDTMP in bone metastatic pain palliation in breast cancer and hormone refractory prostate cancer. Clin Nucl Med. 2013;38:88–92.
16. Pfannkuchen N, Meckel M, Bergmann R, Bachmann M, Bal C, Sathekge M, et al. Novel radiolabeled bisphosphonates for PET diagnosis and endoradiotherapy of bone metastases. Pharmaceuticals. 2017;10:45.
17. Meckel M, Bergmann R, Miederer M, Roesch F. Bone targeting compounds for radiotherapy and imaging: *Me(III)-DOTA conjugates of bisphosphonic acid, pamidronic acid and zoledronic acid. EJNMMI Radiopharm Chem. 2016;1:14.
18. Fellner M, Baum RP, Kubíček V, Hermann P, Lukeš I, Prasad V, et al. PET/CT imaging of osteoblastic bone metastases with 68 Ga- bisphosphonates: first human study. Eur J Nucl Med Mol Imaging. 2010;37:834.
19. Baum RP, Kulkarni HR. Theranostics: from molecular imaging using Ga-68 labeled tracers and PET/CT to personalized radionuclide therapy—the Bad Berka Experience. Theranostics. 2012;2:437–47.
20. Holub J, Meckel M, Kubíček V, Rösch F, Hermann P. Gallium(III) complexes of NOTA-bis (phosphonate) conjugates as PET radiotracers for bone imaging. Contrast Media Mol Imaging. 2015;10:122–34.
21. Bergmann R, Meckel M, Kubíček V, Pietzsch J, Steinbach J, Hermann P, et al. (177)Lu-labelled macrocyclic bisphosphonates for targeting bone metastasis in cancer treatment. EJNMMI Res. 2016;6:5.
22. Ebetino FH, Hogan AML, Sun S, Tsoumpra MK, Duan X, Triffitt JT, et al. The relationship between the chemistry and biological activity of the bisphosphonates. Bone. 2011;49:20–33.
23. Russell RGG. Bisphosphonates. Mode of action and pharmacology. Pediatrics. 2007;119(Supplement 2):150–62.
24. Dalle Carbonare L, Zanatta M, Gasparetto A, Valenti MT. Safety and tolerability of zoledronic acid and other bisphosphonates in osteoporosis management. Drug Healthc Patient Saf. 2010;2:121–37.
25. Pfannkuchen N, Bausbacher N, Pektor S, Miederer M, Rosch F. In vivo evaluation of [^{225}Ac]Ac-DOTA ZOL for α-therapy of bone metastases. Curr Radiopharm. 2018;11:223–30.
26. Passah A, Tripathi M, Ballal S, Yadav MP, Kumar R, Roesch F, et al. Evaluation of bone-seeking novel radiotracer68Ga-NO2AP-Bisphosphonate for the detection of skeletal metastases in carcinoma breast. Eur J Nucl Med Mol Imaging. 2017;44:41–9.
27. Chopra A. 68 Ga-labeled (4-{[(bis(phosphonomethyl))carbamoyl] methyl}-7,10-bis(carboxymethyl)-1,4,7,10-tet raazacyclododec-1-yl)acetic acid (BPAMD). In: Molecular imaging and contrast agent database (MICAD). 2004. http://www.ncbi.nlm.nih.gov/pubmed/23193622. Accessed 27 Dec 2018.
28. Khawar A, Eppard E, Sinnes JP, Roesch F, Ahmadzadehfar H, Kürpig S, et al. [^{44}Sc]Sc-PSMA-617 biodistribution and dosimetry in patients with metastatic castration-resistant prostate carcinoma. Clin Nucl Med. 2018;43:323–30.
29. Stabin MG. Case studies. In: Fundamentals of nuclear medicine dosimetry. New York: Springer; 2008. pp. 119–70.
30. ICRP. Basic anatomical and physiological data for use in radiological protection—the skeleton. ICRP Publication 70. Ann ICRP. 1995;25(2).
31. Hindorf C, Lindén O, Tennvall J, Wingårdh K, Strand SE. Evaluation of methods for red marrow dosimetry based on patients undergoing radioimmunotherapy. Acta Oncol (Madr). 2005;44:579–88.
32. Shen S, DeNardo GL, Sgouros G, O'Donnell RT, DeNardo SJ. Practical determination of patient-specific marrow dose using radioactivity concentration in blood and body. J Nucl Med. 1999;40:2102–6.
33. Sgouros G, Stabin M, Erdi Y, Akabani G, Kwok C, Brill AB, et al. Red marrow dosimetry for radiolabeled antibodies that bind to marrow, bone, or blood components. Med Phys. 2000;27:2150–64.
34. Siegel JA. Establishing a clinically meaningful predictive model of hematologic toxicity in nonmyeloablative targeted radiotherapy: practical aspects and limitations of red marrow dosimetry. CANCER Biother Radiopharm. 2005;20:126–40.
35. Kurdziel KA, Shih JH, Apolo AB, Lindenberg L, Mena E, McKinney YY, et al. The kinetics and reproducibility of ^{18}F-sodium fluoride for oncology using current PET camera technology. J Nucl Med. 2012;53:1175–84.
36. ICRP. Radiation dose to patients from pharmaceuticals-addendum 3 to ICRP publication 53. ICRP publication 106. Ann ICRP. 2008;38:1–2.
37. Walker RC, Smith GT, Liu E, Moore B, Clanton J, Stabin M. Measured human dosimetry of 68 Ga-DOTATATE. J Nucl Med. 2013;54:855–60.
38. Afshar-Oromieh A, Hetzheim H, Kratochwil C, Benesova M, Eder M, Neels OC, et al. The novel theranostic PSMA-ligand PSMA-617 in the diagnosis of prostate cancer by PET/CT: biodistribution in humans, radiation dosimetry and first evaluation of tumor lesions. J Nucl Med. 2015;56:1697–705.
39. Herrmann K, Bluemel C, Weineisen M, Schottelius M, Wester H-J, Czernin J, et al. Biodistribution and radiation dosimetry for a probe targeting prostate-specific membrane antigen for imaging and therapy. J Nucl Med. 2015;56:855–61.